Long-term photometry of the symbiotic nova V1329 Cyg

D.Chochol[1], I.L.Andronov[2], V.P.Arkhipova[3], L.L.Chinarova[2], J.Mattei[4], S.Y.Shugarov[3]

[1] *Astronomical Institute of the Slovak Academy of Sciences 059 60 Tatranská Lomnica, The Slovak Republic*

[2] *Astronomical Observatory, Odessa State University T.G.Shevchenko Park, Odessa 270014, Ukraine*

[3] *Sternberg State Astronomical Institute Universitetskij Prosp. 13, Moscow 119899, Russia*

[4] *American Association of Variable Star Observers, 25 Birch St., Cambridge, MA 02138, USA*

Received: November 10, 1998

Abstract. New UBV photometry of the symbiotic nova V1329 Cyg taken in 1988-97 is presented. Long-term postoutburst UBV photoelectric, photographic and visual observations from the AAVSO and AFOEV databases are discussed. The periodogram analysis using the trigonometric polynomial fit with a linear trend reveals the mean normal epoch of the minimum and the mean best fit period as JD $2446771 \pm 3^{\rm d}$ and $956\overset{\rm d}{.}5 \pm 0\overset{\rm d}{.}6$, respectively. The amplitude of the brightness variations is significantly higher in the U-band ($1\overset{\rm m}{.}6$) than in the B,V and pg bands ($1\overset{\rm m}{.}22$). The largest slope of the mean brightness decrease is in the U-band. The characteristics of the light-curves extremes in different bands are tabulated. The phases of the U,B,V light-curves coincide within the error estimates. A secondary period of $553^{\rm d}$ and a cycle of $\approx 5300^{\rm d}$ are suggested.

Key words: stars – binaries – symbiotic – photometry – V1329 Cyg

1. Introduction

V1329 Cyg (HBV 475) is a member of the small sub-group of symbiotic novae, also including V1016 Cyg and HM Sge, in which TNR outburst leads to a nebular spectrum (Mürset & Nussbaumer, 1994).

In order to illustrate the general photometric behaviour of V1329 Cyg, the historical photographic light-curve (henceforth LC) is presented in Fig. 1. It was compiled using the data published by Dumortier & Stram (1970), Kohoutek & Bossen (1970), Richter (1972), Hicks (1973), Stienon et al. (1974), Witzigman et al. (1978), Iijima et al. (1981), Munari et al. (1988), Arkhipova & Mandel (1991),

Skopal et al. (1992), Hric et al. (1994). In the years 1891-1964 the pg brightness of the object fluctuated around $15^{\rm m}$, with occasional $2\overset{\rm m}{.}5$ deep decreases, which repeated with a period of 950 - 959 days (Stienon et al., 1974; Grygar et al., 1979; Munari et al., 1988). They were explained as the eclipses of a hot component by a red giant. The nova-like outburst of the object started in 1964. The brightness maximum of $11\overset{\rm m}{.}5$ was reached in October 1966. The brightness decline has been accompanied by wave-like variations with the periodicity found in the pre-outbust data. Schild & Schmid (1997) found the ephemerides, valid for the pre-outburst and post-outburst data as $\mathrm{JD}_{min} = 2\ 427\ 687(\pm 20) + 958.0(\pm 1.8)\times E$ and $\mathrm{JD}_{min} = 2\ 444\ 866(\pm 25) + 955(\pm 15)\times E$, respectively. They adopted the ephemeris $\mathrm{JD}_{min} = 2\ 444\ 890 + 956.5\times E$ valid for both sets of data.

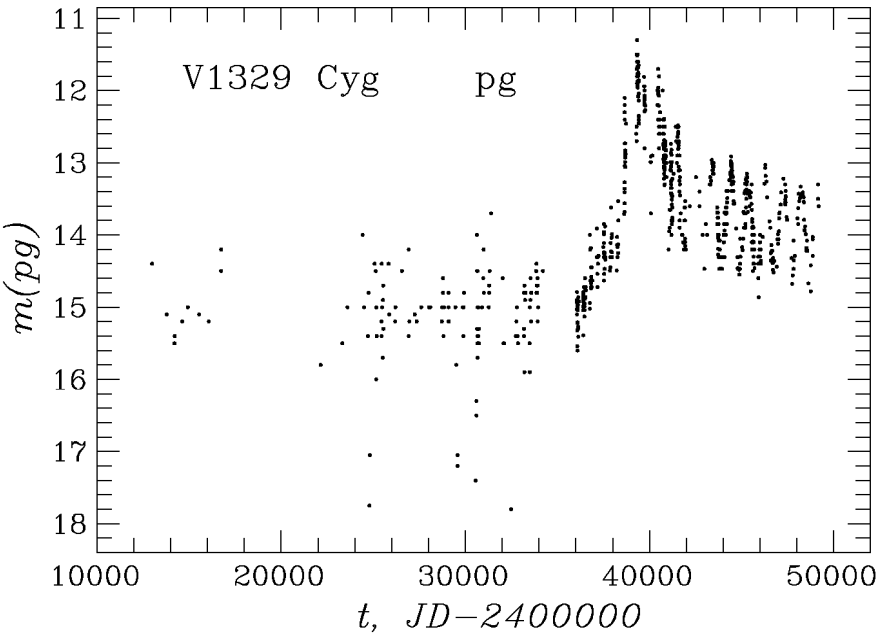

Figure 1. The historical photographic LC compiled from published data.

The aim of our paper is to present a new set of U,B,V observations taken in the years 1988-1997 and to perform the period analysis of the post-outburst UBV photoelectric and photographic observations as well as visual estimates of V1329 Cyg from AFOEV and AAVSO databases.

2. New observations and data-sets used for the analysis

New photoelectric UBV observations of V1329 Cyg were obtained at the Crimean Station of the Sternberg Astronomical Institute in 1988-1997. A single-channel,

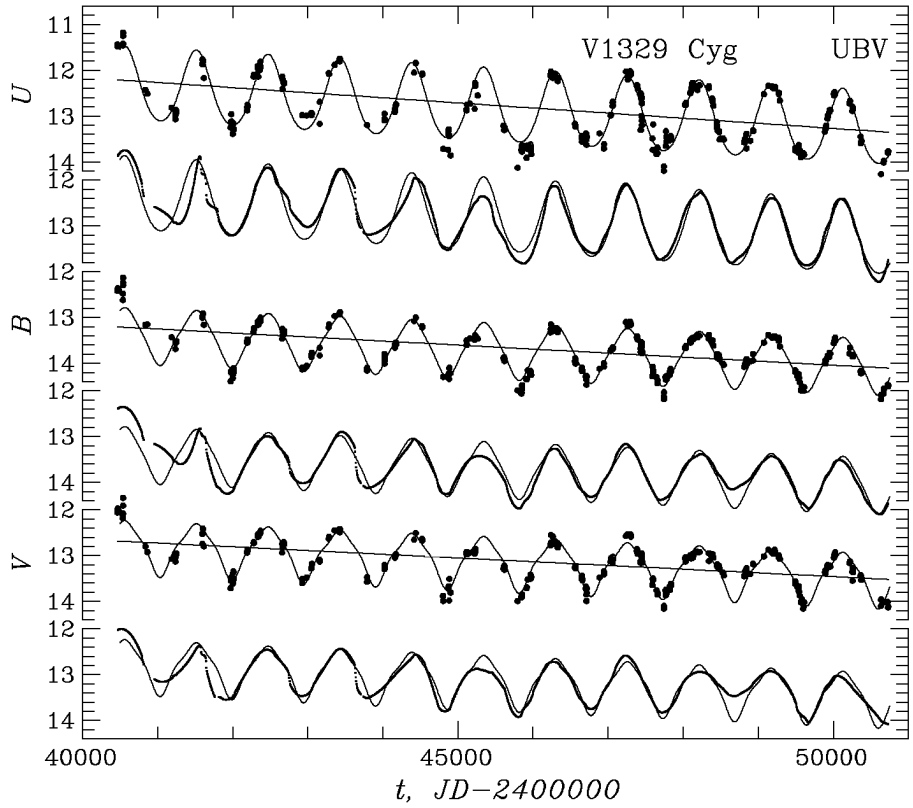

Figure 2. The UBV LCs (points) and their approximations by a trigonometric polynomial of order $s = 2$ including a linearly decreasing trend (thin curve) calculated for the data after JD 24420000. The thick curve shows the running parabola (RP) fit with $\Delta t = 400^{\rm d}$ for all data. The declining straight lines show the linear fits using all data.

pulse-counting, photoelectric photometer installed in the Cassegrain focus of the 0.6 m reflector was used. The star BD +35° 4300 (V=9.71, B=9.91, U=10.13) served as the comparison star. Data reduction and atmospheric extinction corrections were carried out in the usual way. As this instrumental system is nearly in agreement with the standard UBV system, the transformation to this system is not necessary (Arkhipova, 1977). Our photoelectric observations taken on 148 nights between Aug. 7, 1988 and Oct. 8, 1997 are in Tab. 6. The U,B,V magnitudes are normal points - mean night averages of the individual observations taken 2-3 times during the night. The mean error of one normal point is $0\overset{\rm m}{.}01$ in B and V and $0\overset{\rm m}{.}02$ in U.

U,B,V LCs of V1329 Cyg compiled from our data as well as data published by Kohoutek & Bossen (1970), Bossen (1972), Arkhipova & Mandel (1973), Arkhipova (1977), Gravina (1985), Taranova & Yudin (1986), Arkhipova & Ikon-

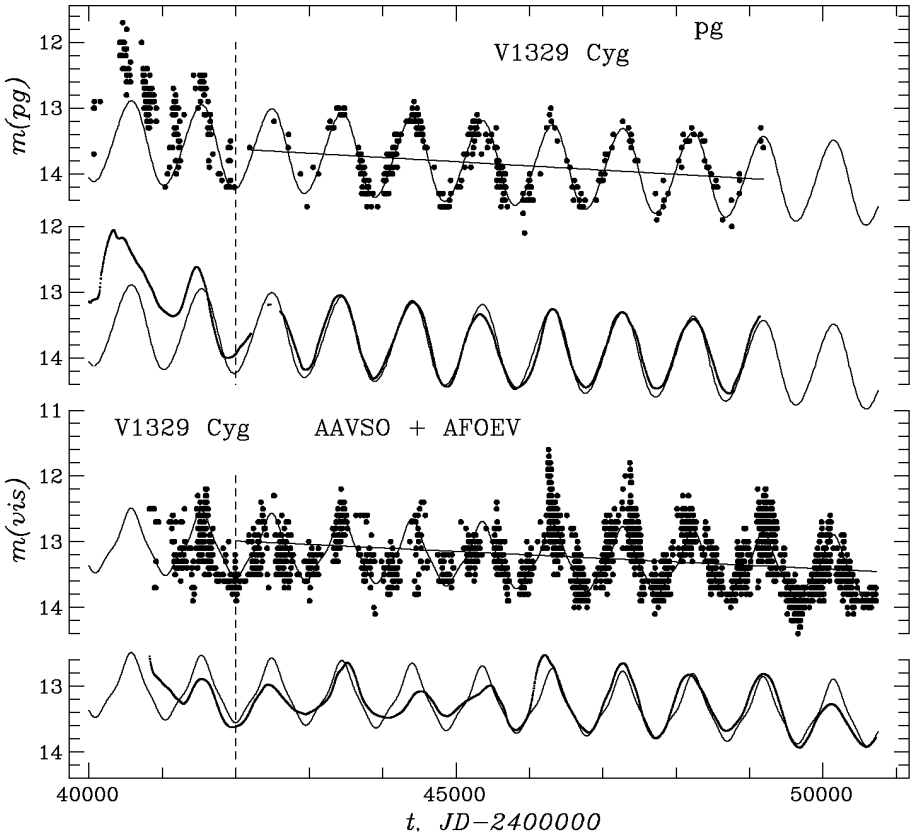

Figure 3. The pg and visual LCs (points) and their approximations by a trigonometric polynomial of order $s = 2$ and a linearly decreasing trend (thin curve) calculated for the data after JD 2442000 (vertical dashed line). The thick curve shows the running parabola (RP) fit with $\Delta t = 400^{\mathrm{d}}$. The declining straight lines show the linear fits.

nikova (1989), Dapergolas et al. (1991) are shown in Fig. 2.

Visual data consisted of 3173 and 2323 observations from the AAVSO and AFOEV (Schweitzer, 1997) databases, respectively. A significant part of the data overlapped, being published in both databases. After removing the "duplicates", "unsure" (:) and "fainter than" (<) data, a total of 4024 original visual (vis) estimates remained. As shown in Fig. 3, the photographic and visual LCs of V1329 Cyg are characterized by a rapid decline with some superimposed outbursts before JD 2442000. After this date, the mean slope decreased and the LCs started to exhibit wave-like periodic variations. The number of "post-outburst" points after this date is $n = 3754$.

Long-term, post-outburst U,B,V photoelectric, photographic and visual light curves were analyzed in detail. The characteristics of the runs: the times of

the first and last observations (in JD–2400000), the number of observations, the range, the sample mean, and the standard deviation from the mean, are summarized in Table 1.

Table 1. The characteristics of the data sets in different runs

band	t_1	t_n	n	range	$\langle m \rangle$	σ_O
U	40467	50730	345	$11\overset{m}{.}2$-$14\overset{m}{.}3$	$12\overset{m}{.}86$	$0\overset{m}{.}67$
B	40467	50730	350	$12\overset{m}{.}1$-$14\overset{m}{.}8$	$13\overset{m}{.}72$	$0\overset{m}{.}50$
V	40467	50730	351	$11\overset{m}{.}7$-$14\overset{m}{.}2$	$13\overset{m}{.}16$	$0\overset{m}{.}47$
pg	12994	49184	943	$11\overset{m}{.}3$-$17\overset{m}{.}8$	$13\overset{m}{.}82$	$1\overset{m}{.}00$
vis	40823	50722	4024	$11\overset{m}{.}6$-$14\overset{m}{.}4$	$13\overset{m}{.}28$	$0\overset{m}{.}44$

3. Periodogram analysis with trend

Due to the fact that a slow trend is superimposed on the cyclic luminosity variations, the problem of the period search becomes more complicated. Assuming a polynomial shape of the trend of order n_p, one may write an expression

$$m(\bar{t}+\tau) = a_1 + \sum_{k=1}^{s}(a_{2k}\sin(2\pi f k\tau) + a_{2k+1}\cos(2\pi f k\tau)) + \sum_{k=1}^{q} a_{2s+1+k}\tau^k. \quad (1)$$

Here we introduce the variable $\tau = t - \bar{t}$ ($\bar{t}$ is the mean of the times of observations) to decrease the degeneracy of the matrix of normal equations (cf. Andronov, 1994). For the fixed frequency f and the degrees s and q of the trigonometric and ordinary polynomial, respectively, the parameters a_k, $k = 1, ...1 + 2s + q$ may be obtained by the least squares method. This is a statistically justified method because all these parameters are determined from a joint system of normal equations.

Another approach is to determine the parameters of the trend and then to search for periodicity in the $O - C$ residuals from the trend. Such a process is similar to "prewhitening" (Wehlau and Leung, 1964). As an example, we have computed the results of the fits for all photoelectric B observations. The linear trend may be written as

$$m_B = \underset{\pm 2}{13\overset{m}{.}71} + \underset{\pm 8}{88\times 10^{-6}}\ (t - 46280). \quad (2)$$

The sine approximations for the original observations "O" and their residuals "$O - C$" from a linear fit (2) correspond to the period $P = 960\overset{d}{.}8 \pm 1\overset{d}{.}6$ "O" ($955\overset{d}{.}7 \pm 0\overset{d}{.}9$ "$O - C$"), mean $a_1 = 13\overset{m}{.}76 \pm 0\overset{m}{.}01$ ($0\overset{m}{.}02 \pm 0\overset{m}{.}01$), semiamplitude $r = 0\overset{m}{.}62 \pm 0\overset{m}{.}02$ ($0\overset{m}{.}57 \pm 0\overset{m}{.}01$) and the normal epoch for minimum $JD_{min} = 2446767 \pm 5$ (2446777 ± 2). The parameters of the complete fit (1) coincide with

that of the prewhitened solution within their error estimates: $P = 956\overset{\mathrm{d}}{.}4 \pm 2\overset{\mathrm{d}}{.}6$, $r = 0\overset{\mathrm{m}}{.}59 \pm 0\overset{\mathrm{m}}{.}01$, $JD_{min} = 2446777 \pm 3$, $a_1 = 13\overset{\mathrm{m}}{.}75 \pm 0\overset{\mathrm{m}}{.}01$. This occurs because ≈ 10 cycles are covered by the data and thus the phases of the observations are distributed relatively homogeneously. However, the linear trend term $a_{2s+2} = (77 \pm 3)\ 10^{-6}$ mag/day in a complete fit differs from the simple linear slope by 14%, and for other data up to $\approx 40\%$.

One may note that the moment of minimum for a sinusoidal wave is shifted compared to a minimum of the "sine+line" function. This shift for V1329 Cyg is $\Delta T_{min} = 1\overset{\mathrm{d}}{.}5$ and is smaller than the statistical error estimates. These errors are much larger for the sine fit of the original data, as the trend disturbs the phase curve.

The residuals of the original data from a best sine fit show a well pronounced trend. However, its value $(72 \pm 3)\ 10^{-6}$ mag/day differs from the fit (2) by 22%. Thus one has to use a complete set of $1 + 2s + q$ equations instead of two sets of equations with $1 + q$ and $1 + 2s$ unknowns. This example shows a bias of the results owed to incomplete models and thus it may be recommended to use high-order models instead of step-by-step "prewhitening".

The best trigonometric polynomial fit with a linear trend was computed for the U,B,V, vis, pg and pg+B data. The trend is close to the linear one not for the complete data set, but for the "post-outburst" data after the stage of rapid decrease of brightness, i.e. after JD 2442000. The parameters of the fits for such restricted data are listed in Table 2. Here the degree of the polynomial trend was set to $q = 1$. The degree of the trigonometric polynomial s (different for each data set) was determined by using the Fischer's criterion with a "false alarm" probability $P_r < 10^{-4}$. This is the probability that the $(s-1)$ -th harmonic of a given amplitude may be obtained, suggesting the signal is a white noise. The value of P_r may be determined by using the equation $P_r(s) = (1 - V_B)^{\eta}$, where $\eta = (n-3-2s-q)/2$, $V_B = 1-\Sigma[s]/\Sigma[s-1]$ and $\Sigma[s]$ is the sum of squares of the residuals from the trigonometric polynomial of order s with the q-th order trend. This expression generalizes that of Andronov (1994) for non–zero values of q. For a fixed s, the periodogram may be computed as $S(f) = \sigma_C^2/\sigma_O^2$, where σ_O^2 and σ_C^2 are variances of the original data and the smoothed values at the arguments of observations, respectively. The term a_{2s+2}, measured in magnitudes per day, corresponds to a linear trend. The normal epochs T_{max}, T_{min} are expressed in JD-2400000. The pg system is close to the B system, thus it is natural to join the "pg+B" data to obtain the longest possible data-set. However, there is a systematic shift $\langle pg - B \rangle = 0\overset{\mathrm{m}}{.}10$, which was taken into account to reduce the B data to the pg system. This shift was determined by comparing the original pg data with a smoothed value of the B LC at corresponding times and vice versa. The smoothing function was obtained by using a "running parabola" fit with an optimal value of the filter half-width $\Delta t = 400^{\mathrm{d}}$ (see Section 4 for a description).

The periodograms for the B data after JD 2442000 are shown in Fig. 4. Run 1 was obtained by removing the linear trend. The highest peak at the periodogram

Table 2. Characteristics of the trigonometric polynomial fit with a linear trend for the observations after JD 2442000

	U	B	V	vis	pg	pg+B
n	314	319	320	3754	392	711
$\bar{t}$	46785	46779	46766	47726	45230	45925
a_1	12.95	13.79	13.21	13.34	13.82	13.76
$\pm$	0.01	0.01	0.01	0.01	0.01	0.01
s	2	3	3	3	2	2
$10^6 a_{2s+2}$	100	68	70	42	64	108
$\pm$	4	3	3	2	5	7
P	953.9	956.0	957.8	956.3	958.9	958.2
$\pm$	3.9	2.5	2.4	1.9	4.8	6.4
T_{max}	46300.0	46304.3	46298.3	46315.0	46362.2	46328.8
$\pm$	3.9	6.2	5.8	3.2	5.7	5.2
T_{min}	46778.9	46771.7	46768.0	46778.9	46762.1	46755.5
$\pm$	10.5	4.5	3.3	4.9	5.8	4.5
$M-m$	0.498	0.511	0.510	0.515	0.540	0.555
$\pm$	0.014	0.006	0.006	0.005	0.011	0.009
Δm	1.598	1.234	1.211	1.007	1.260	1.269
$\pm$	0.022	0.018	0.017	0.013	0.019	0.016
σ_{O-C}	0.170	0.107	0.105	0.275	0.151	0.134

corresponds to $P = 955\overset{\mathrm{d}}{.}7 \pm 1\overset{\mathrm{d}}{.}0$, the value close to that listed in Table 2. Run 2 was computed as the difference between run 1 and the sine fit ($s = 1$, $q = 0$), i.e. consequently prewhitened to a linear trend and a 956^{d} wave. Run 3 was computed as the difference between run 1 and the trigonometric polynomial fit with a statistically significant order $s = 3$. The periodograms of runs 2 and 3 show two prominent peaks at $5300^{\mathrm{d}} \pm 160^{\mathrm{d}}$ ($S(f) = 0.22$ and 0.26, respectively) and $554^{\mathrm{d}} \pm 2^{\mathrm{d}}$ ($S(f) = 0.26$ and 0.26, respectively). The secondary peak is shifted from 581^{d} for run 1 to 555^{d} and 553^{d} for runs 2 and 3, respectively. One may note the significant difference between the values obtained for different runs at the same wavelength that justifies the usage of complete system of the equations (1) instead of step–by–step "prewhitening". The ephemeris for the maximum of the 553^{d} wave is

$$JD_{max} = \underset{\pm 9}{2446711} + \underset{\pm 1\overset{\mathrm{d}}{.}9}{553\overset{\mathrm{d}}{.}1} \times E, \qquad (3)$$

The corresponding phase diagram is shown on Fig. 5. The O-C deviations prewhitened to a linear trend, trigonometric polynomial and a best sine fit with $553\overset{\mathrm{d}}{.}1$ period are depicted on Fig. 6. The 5300^{d} wave is clearly visible. Similar results may be seen in the periodograms for other bands. The mean values and

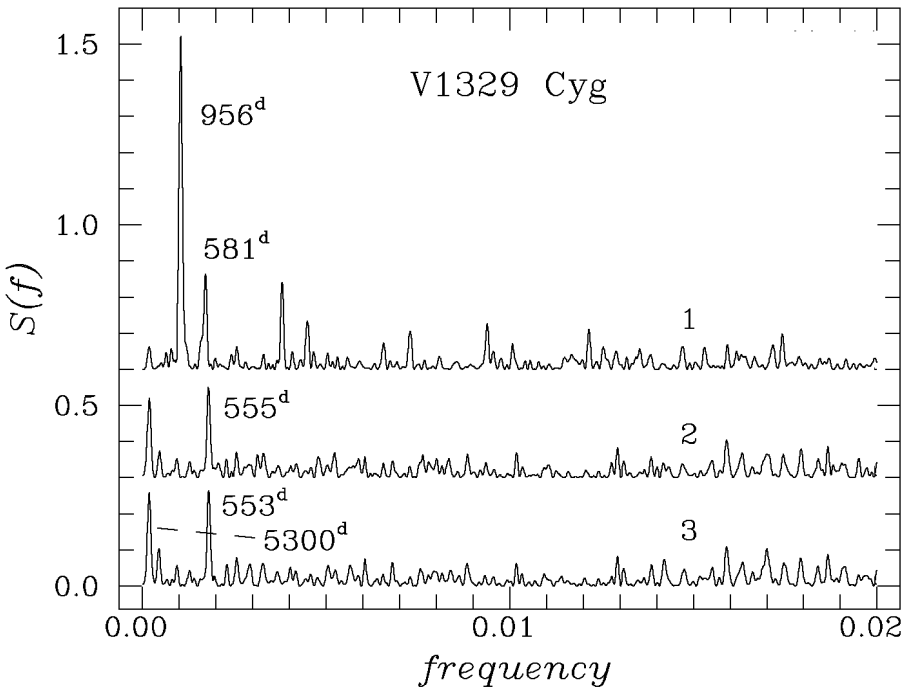

Figure 4. The periodograms $S(f)$ for the residuals from the linear "$s = 0$, $q = 1$" fit (1), from the data prewhitened consecutively in respect to the linear trend and best harmonic ($s = 1$) fit (2) and to the best trigonometric polynomial ($s = 3$) fit with a linear trend (3). The periodograms are shifted with a step of 0.3. The photoelectric B observations after JD 2442000 are used.

standard errors in both figures were computed by sampling the data in intervals of equal length.

The semi–amplitude of $554^{\rm d}$ wave in U,B and V is equal to $0\overset{\rm m}{.}075 \pm 0\overset{\rm m}{.}007$, $0\overset{\rm m}{.}077 \pm 0\overset{\rm m}{.}007$ and $0\overset{\rm m}{.}069 \pm 0\overset{\rm m}{.}007$, respectively. Corresponding values of $S(f)$ and L_p are 0.100, 0.264, 0.234 and 4.9, 18.8, 16.0, respectively. The "false alarm" probability is equal to 10^{-L_p} (cf. Andronov, 1994). Thus one may conclude that the effective amplitude of such a secondary wave is nearly the same in all bands, but its contribution to U is much smaller than in other bands. The variability is most probably attributed to the hot component, because J,H,K,L photometry do not exhibit clear variational patterns (Nussbaumer & Vogel, 1991). The $554^{\rm d}$ and $5300^{\rm d}$ waves could be explained by systematic changes in both geometry and location of the HII region, which is the main source of the optical continuum as proposed by Skopal (1998).

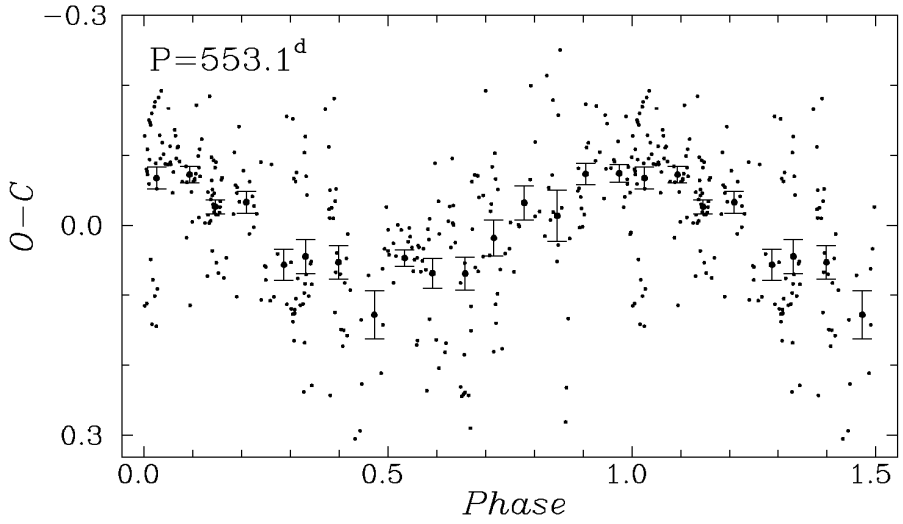

Figure 5. The phase diagram for B run 3 according to the ephemeris: $JD_{max} = 2446711 + 553.1 \times E$.

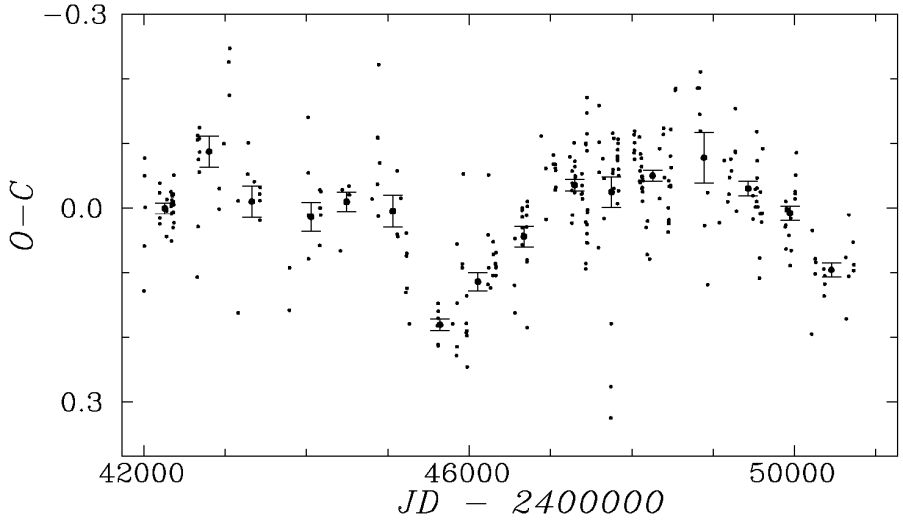

Figure 6. The $O-C$ deviations of the post-outburst B data consequently prewhitened to a linear trend and a trigonometric polynomial and to a best sine fit with $553^{d}.1$ period.

4. The running parabolae fit and characteristics of individual cycles

As the individual cycles of variability may change their shape, we have used the method of running parabolae introduced by Andronov (1990) and recently extended to arbitrary basic and weight functions by Andronov (1997). For the fixed set of these functions, the only free parameter is the filter half–width Δt which must be determined by computing the effective parameters of the fit for a grid of Δt. We have computed the error estimates σ_1 of the accuracy of one observation, (σ_4 ($= R\sigma_1$) in the notation of Andronov (1997)) and the signal to noise ratio S/N, which is equal to σ_C/σ_4. Here σ_C is the r.m.s. deviations of the smoothed values from the mean.

Besides these parameters, Fig. 7 shows the dependencies of σ_2, $\sigma_5 = R\sigma_2$ (other estimates of σ_1 and σ_4, see Andronov (1997) for details), R and $\sigma_3 = \sigma_{O-C}$ on Δt. One may note that the maximum of S/N occurs at $\Delta t = 400^{\rm d}$, just where σ_4 reaches its minimum (neglecting differences of a few percent which are not very important for the fit). This value of Δt is slightly smaller than that $0.545P = 521^{\rm d}$ expected for the harmonic signal with uncorrelated noise (Andronov, 1997). This is usual for signals with significant contributions of the harmonics of the main wave ($s > 1$) or for the signals with variable shape.

The two estimates σ_1 and σ_2 are very close to each other, justifying their good accuracy. The biased error estimate σ_3 is much smaller than σ_1 and σ_2 for small Δt, because of a smaller effective number of observations n_e used for the local fit than for the larger Δt. The parameter R monotonously decreases with Δt as n_e increases. All the parameters become asymptotically constant at Δt exceeding the length of the interval of observations.

The corresponding dependencies for other bands show similar shapes and the values of Δt corresponding to the maximal S/N differ from the adopted value by a few percent, thus there is no need to use different values of Δt for different data. The main characteristics for $\Delta t = 400^{\rm d}$ are listed in Table 3.

Table 3. Error estimates of the data σ_1, the fit σ_4 and the S/N ratio for different data sets

	U	B	V	pg	vis	AAVSO	AFOEV
σ_1	$0\overset{\rm m}{.}138$	$0\overset{\rm m}{.}078$	$0\overset{\rm m}{.}085$	$0\overset{\rm m}{.}189$	$0\overset{\rm m}{.}242$	$0\overset{\rm m}{.}234$	$0\overset{\rm m}{.}224$
σ_4	$0\overset{\rm m}{.}046$	$0\overset{\rm m}{.}026$	$0\overset{\rm m}{.}028$	$0\overset{\rm m}{.}039$	$0\overset{\rm m}{.}023$	$0\overset{\rm m}{.}025$	$0\overset{\rm m}{.}027$
S/N	14.0	19.1	16.3	14.8	15.8	14.9	14.5

Here we also include the sets from the AAVSO and AFOEV databases separately. As expected, the difference between the values of σ_1 is not very large (only 5%). The difference of σ_4 owes to the difference of n_e. However, it is strange that the "vis" data set, which is the unoverlapped sum of the AAVSO and AFOEV databases, corresponds to a larger value of σ_1. As an explanation,

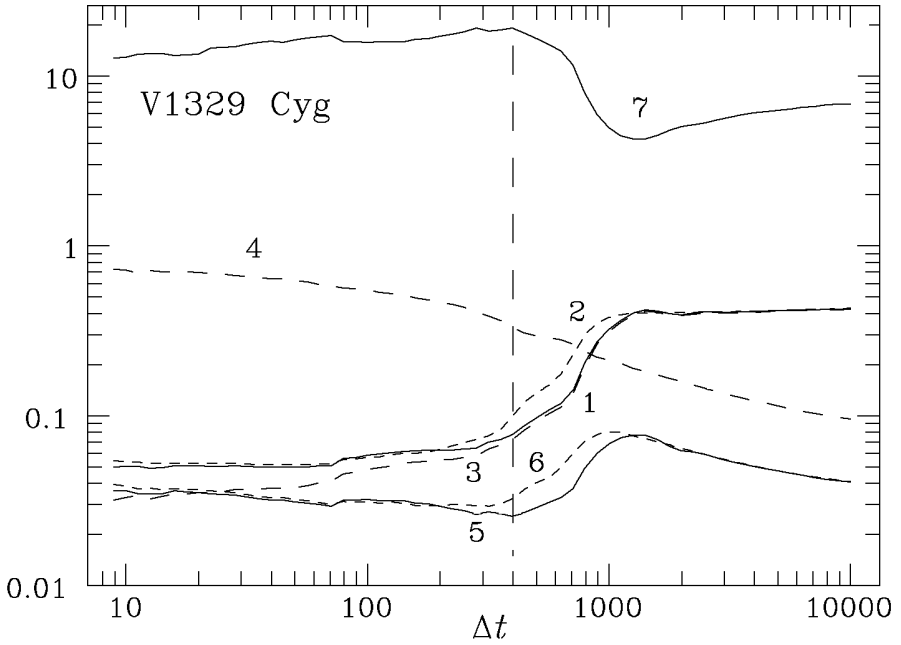

Figure 7. The dependence of the characteristics of the running parabola (RP) fit for the photoelectric B observations on Δt. The vertical line corresponds to the position of the local maximum at the S/N curve: $\Delta t = 400^{\rm d}$. The lines correspond to: 1 (σ_1), 2 (σ_2), 3 ($\sigma_3 = \sigma_{O-C}$), 4 (R), 5 ($\sigma_4 = R\sigma_1$), 6 ($\sigma_5 = R\sigma_2$), 7 ($S/N = \sigma_C/\sigma_4$).

one may suggest the differences between the sequences of the comparison stars. However, this value is 10% smaller than for other stars, thus the data is of relatively low scatter.

The photographic data shows a larger value of σ_1 than that of the photoelectric observations because of their lower accuracy. However, the scatter is smaller than in the visual data because of the better homogeneity of the material used.

The characteristics of the extremes, determined by the method of running parabolae with the adopted filter half–width $\Delta t = 400^{\rm d}$ are listed in Tables 4 and 5. To compute the phases, we have used the ephemeris

$$JD_{min} = \underset{\pm 3}{2446771} + \underset{\pm 0.^{\rm d}6}{956.^{\rm d}5} \times E. \qquad (4)$$

The normal epoch of minimum and the period were computed as mean values from the values listed in Table 2 for U, B, V, vis and pg with weights proportional to inverse squares of the corresponding statistical errors, as usually assumed for the weighted mean (cf. Whittaker & Robinson 1926).

One may note in Figs. 2 and 3 the large deviations of the LC from the trigonometric polynomial trend before JD 2442000, where the fast decline and

Table 4. The U,B,V,pg extremes: time T_e (-2400000), phase ϕ_e and magnitude m_e

T_e	ϕ_e	m_e	T_e	ϕ_e	m_e
	U Max			U Min	
40563 ±21	0.509±0.022	11.34±0.05	41276±28	0.255±0.029	12.96±0.05
41562 ± 4	0.554±0.004	11.48±0.19	41974± 8	-0.015±0.008	13.21±0.05
42467 ± 4	0.500±0.004	11.73±0.03	42996±17	0.053±0.018	13.02±0.06
43452 ± 4	0.530±0.005	11.75±0.04	43815± 7	-0.091±0.008	13.20±0.04
44422 ± 5	0.544±0.005	11.95±0.04	44865±15	0.008±0.016	13.52±0.08
45326 ±18	0.490±0.018	12.35±0.11	45871±13	0.059±0.014	13.82±0.04
46286 ±11	0.493±0.011	12.13±0.03	46808±22	0.038±0.023	13.59±0.05
47233 ± 6	0.483±0.007	12.08±0.05	47680±25	-0.050±0.026	13.74±0.06
48227 ± 2	0.522±0.002	12.26±0.03	48641±10	-0.045±0.011	13.80±0.05
49176 ±12	0.514±0.012	12.39±0.03	49638±18	-0.003±0.019	13.86±0.02
50098 ± 4	0.478±0.004	12.41±0.03	50604± 7	0.008±0.007	14.22±0.05
	B Max			B Min	
40539 ±61	0.485±0.064	12.35±0.06	41306±26	0.287±0.028	13.61±0.07
41564 ± 6	0.557±0.007	12.82±0.13	41931±10	-0.060±0.011	14.25±0.03
42462 ± 5	0.495±0.005	12.99±0.02	42936±36	-0.010±0.038	14.02±0.05
43450 ± 3	0.528±0.003	12.90±0.02	43808±22	-0.098±0.023	14.12±0.05
44416 ± 2	0.537±0.002	13.05±0.03	44837± 4	-0.022±0.004	14.26±0.03
45269 ±31	0.430±0.033	13.42±0.02	45814± 5	-0.000±0.005	14.57±0.04
46282 ±12	0.489±0.013	13.27±0.02	46771± 9	-0.000±0.009	14.32±0.03
47234 ± 5	0.484±0.005	13.16±0.02	47697±12	-0.032±0.012	14.38±0.03
48233 ± 2	0.528±0.002	13.38±0.01	48652±11	-0.033±0.012	14.15±0.02
49172 ±11	0.510±0.011	13.43±0.02	49670± 2	0.031±0.002	14.58±0.04
50080 ± 8	0.459±0.008	13.51±0.03	50620± 6	0.024±0.006	14.70±0.03
	V Max			V Min	
40517 ±74	0.462±0.077	12.00±0.04	41065±31	0.034±0.033	13.16±0.10
41554 ±14	0.546±0.015	12.37±0.26	41910±19	-0.082±0.020	13.55±0.04
42458 ± 5	0.491±0.006	12.46±0.02	42919±31	-0.027±0.033	13.47±0.05
43442 ± 3	0.519±0.003	12.44±0.02	43783± 9	-0.124±0.009	13.51±0.04
44435 ± 9	0.558±0.010	12.56±0.02	44829± 8	-0.030±0.009	13.80±0.06
45252 ± 6	0.412±0.006	12.86±0.02	45806± 3	-0.009±0.003	13.92±0.02
46266 ±14	0.472±0.015	12.72±0.02	46772±11	0.001±0.012	13.75±0.04
47232 ± 5	0.482±0.006	12.58±0.03	47719±12	-0.009±0.013	13.83±0.03
48219 ±68	0.514±0.071	12.94±0.01	48682± 8	-0.002±0.009	13.47±0.03
49157 ±12	0.494±0.013	12.92±0.02	49669± 2	0.030±0.002	14.05±0.05
50050 ±12	0.428±0.012	13.03±0.03		pg Min	
	pg Max		40019± 6	-0.059±0.006	13.16±0.19
39323± 4	0.213±0.004	11.83±0.06	41138±44	0.111±0.046	13.37±0.06
40334±13	0.270±0.013	12.05±0.13	41887±86	-0.106±0.089	14.00±0.07
41466±11	0.454±0.011	12.62±0.07	42950±48	0.006±0.050	14.18±0.14
43423± 8	0.499±0.008	13.05±0.02	43874± 4	-0.028±0.004	14.32±0.04
44414± 6	0.536±0.007	13.15±0.02	44879± 8	0.022±0.008	14.44±0.02
45323± 8	0.486±0.008	13.34±0.04	45822±14	0.008±0.015	14.46±0.05
46312±10	0.520±0.010	13.26±0.09	46770± 8	-0.001±0.009	14.45±0.04
47265±12	0.517±0.012	13.31±0.04	47733±32	0.006±0.034	14.47±0.05
48229± 9	0.525±0.010	13.41±0.04	48722±19	0.039±0.020	14.54±0.08

Table 5. The extremes based on the visual data: time T_e (-2400000), phase ϕ_e and magnitude m_e

T_e	ϕ_e	m_e	T_e	ϕ_e	m_e
	vis Max			vis Min	
41533±18	0.524±0.019	12.89±0.03	41288± 8	0.268±0.009	13.27±0.04
42442±17	0.474±0.017	12.98±0.05	41948±10	-0.042±0.011	13.62±0.02
43518± 5	0.599±0.005	12.64±0.04	42948±16	0.003±0.017	13.43±0.04
44528±47	0.655±0.049	13.08±0.07	44071±41	0.177±0.043	13.48±0.03
45469± 8	0.639±0.009	12.99±0.03	44878±15	0.021±0.016	13.45±0.03
46210± 5	0.414±0.005	12.53±0.03	45814±10	-0.000±0.010	13.67±0.03
47275± 5	0.527±0.005	12.65±0.03	46811± 6	0.042±0.006	13.71±0.02
48182± 7	0.475±0.007	12.82±0.02	47719± 6	-0.009±0.007	13.79±0.02
49191± 9	0.530±0.009	12.81±0.02	48681±11	-0.003±0.011	13.68±0.02
50112± 6	0.493±0.006	13.27±0.02	49679± 3	0.040±0.004	13.93±0.01
			50590± 5	-0.007±0.005	13.92±0.01

frequent outbursts were replaced by a relatively smooth curve with much smaller trend. Also, there are large distortions of the smoothing curve during the gaps causing apparent shifts of the extremes, e.g. near JD 2441300. The U and B LCs are highly distorted; the more dense photographic data shows an outburst that also shifts the LC.

However, the visual observations show much larger deviations from the periodic fit causing apparent huge changes to the shape of the light curve. One may note large apparent visual brightenings near JD 2446259 and 47368, despite the fact that photographic and photoelectric data show no evidence for them. This may be a result of the inhomogeneity of the observations and thus their larger scatter.

To look for possible phase shifts between the LCs in U,B,V bands we have chosen the extremes (either maxima or minima) determined in all three bands, neglecting those seen in one or two bands, only. The accuracy estimates of single data σ were used for the weights $w = \sigma^{-2}$ (e.g. Whittaker & Robinson, 1926). The mean weights of the timings of the extremes correspond to $\sigma_t = 10\overset{\mathrm{d}}{.}7$, $5\overset{\mathrm{d}}{.}1$ and $4\overset{\mathrm{d}}{.}3$ for the U,B and V data, respectively. The weight of each difference was set to $w = w_1 w_2/(w_1 + w_2)$, because the variance of the difference between two uncorrelated variables is equal to the sum of the variances of these variables: $\sigma^2 = \sigma_1^2 + \sigma_2^2$ (e.g. Whittaker & Robinson, 1926). Here the indices 1 and 2 correspond to two colours in a pair. The mean differences between the times of extremes in different colours are $\langle t_U - t_B \rangle = 25^{\mathrm{d}} \pm 11^{\mathrm{d}}$, $\langle t_U - t_V \rangle = 30^{\mathrm{d}} \pm 16^{\mathrm{d}}$ and $\langle t_B - t_V \rangle = 12^{\mathrm{d}} \pm 5^{\mathrm{d}}$. A maximum near JD 2441280 was not taken into account as it was poorly defined. Thus one may conclude that all differences between the times of minima in different colours are equal to zero within corresponding error estimates.

Table 6. Photoelectric UBV observations of V1329 Cyg obtained at the Crimean station of the Sternberg Astronomical Institute.

JD-2400000	U	B	V	JD-2400000	U	B	V
47381	12.34	13.43	12.89	48119	12.30	13.46	12.97
47384	12.33	13.41	12.86	48121	12.36	13.47	12.99
47387	12.36	13.44	12.94	48124	12.35	13.48	13.02
47389	12.34	13.46	12.90	48127	12.31	13.47	13.05
47392	12.40	13.48	12.96	48128	12.30	13.45	13.02
47434	12.60	13.56	12.97	48129	12.28	13.45	13.00
47436	12.51	13.57	12.99	48131	12.29	13.48	12.99
47446	12.59	13.56	12.96	48133	12.29	13.46	13.00
47447	12.58	13.54	12.95	48134	12.33	13.44	12.99
47448	12.61	13.60	13.03	48176	12.38	13.41	12.91
47449	12.72	13.63	13.00	48188	12.43	13.43	12.93
47588	13.49	14.28	13.64	48193	12.36	13.37	12.92
47594	13.74	14.08	13.51	48218	12.33	13.40	12.92
47598	-	14.15	13.53	48340	12.39	13.38	12.95
47599	13.18	14.20	13.50	48341	12.35	13.46	13.12
47644	13.83	14.31	13.76	48387	12.62	13.50	13.01
47656	13.81	14.43	13.85	48390	12.67	13.50	12.97
47657	13.69	14.37	13.81	48400	12.77	13.61	13.04
47765	-	14.30	13.76	48446	13.13	13.86	13.21
47766	13.65	14.36	13.87	48448	13.20	13.83	13.22
47768	13.33	14.35	13.82	48450	13.20	13.86	13.23
47776	13.56	14.36	13.74	48451	13.23	13.80	13.19
47777	13.46	14.28	13.82	48452	13.26	13.87	13.22
47821	13.53	14.25	13.75	48456	13.29	13.88	13.24
47823	13.46	14.17	13.66	48459	13.32	13.84	13.26
47824	13.48	14.17	13.70	48473	13.35	13.85	13.24
47825	13.48	14.17	13.66	48474	13.35	13.90	13.25
47826	13.49	14.15	13.66	48476	13.33	13.91	13.25
47829	13.45	14.13	13.65	48478	13.34	13.83	13.23
47830	13.50	14.12	13.64	48483	13.51	13.91	13.29
47835	13.44	14.15	13.62	48532	13.49	14.01	13.37
47836	13.50	14.18	13.66	48539	13.51	14.04	13.43
47838	13.51	14.15	13.63	48809	13.57	14.08	13.45
48027	12.74	13.67	13.04	48827	13.49	14.00	13.34
48028	12.76	13.64	13.06	48834	13.54	14.01	13.32
48030	12.76	13.66	13.08	48840	13.71	14.01	13.37
48032	12.75	13.67	13.13	48842	13.39	13.91	13.28
48034	12.74	13.64	13.10	48892	13.54	13.96	13.40
48035	12.71	13.62	13.07	48930	13.31	13.80	13.18
48092	12.49	13.49	12.99	48931	13.33	13.94	13.19
48095	12.50	13.55	12.99	49075	12.52	13.55	13.02
48100	12.46	13.52	13.00	49134	12.34	13.38	12.87
48103	12.45	13.53	13.06	49178	12.35	13.44	12.94
48105	12.40	13.48	12.99	49194	12.39	13.44	12.94
48118	12.28	13.45	12.97	49200	12.39	13.42	12.96

Table 6 (continued)

JD-2400000	U	B	V	JD-2400000	U	B	V
49215	12.40	13.41	12.87	49920	13.05	13.86	13.21
49223	12.37	13.44	12.92	49925	12.99	13.84	13.22
49270	12.49	13.50	13.03	49931	13.00	13.86	13.23
49273	12.52	13.44	12.99	49945	12.92	13.86	13.23
49274	12.49	13.51	13.03	49950	12.87	13.77	13.22
49287	12.66	13.63	13.07	49959	12.87	13.79	13.24
49490	13.70	14.15	13.56	50006	12.51	13.56	13.04
49491	13.75	14.19	13.61	50009	12.55	13.54	13.00
49517	13.72	14.25	13.65	50010	12.49	13.54	13.01
49520	13.69	14.29	13.69	50014	12.48	13.50	13.02
49534	13.74	14.34	13.68	50023	12.51	13.44	12.93
49536	13.63	14.24	13.67	50211	12.72	13.79	13.16
49538	13.70	14.32	13.75	50220	12.67	13.66	13.13
49539	13.81	14.34	13.77	50253	12.89	13.82	13.35
49542	13.74	14.31	13.78	50255	12.80	13.85	13.55
49549	13.74	14.41	13.87	50256	12.82	13.83	13.28
49567	13.90	14.59	14.02	50260	12.84	13.85	13.36
49570	13.88	14.57	14.02	50361	13.45	14.17	13.44
49578	13.81	14.53	13.94	50364	13.59	14.22	13.43
49582	-	14.51	13.97	50371	13.55	14.22	13.53
49596	13.84	14.60	14.16	50372	13.54	14.21	13.49
49601	13.81	14.60	14.12	50631	14.27	14.69	14.10
49609	13.84	14.52	14.02	50635	14.27	14.78	13.96
49886	13.34	14.00	13.36	50641	14.06	14.64	13.95
49891	13.29	13.98	13.39	50667	14.02	14.66	14.01
49892	13.29	13.94	13.34	50669	13.98	14.56	14.02
49896	13.28	14.00	13.36	50721	13.79	14.47	14.01
49901	13.21	13.92	13.30	50726	13.81	14.50	14.13
49902	13.25	13.92	13.30	50730	13.77	14.48	14.11

5. Conclusions

1. The ephemeris $\mathrm{JD}_{min} = 2\,446\,771(\pm 3) + 956\overset{\mathrm{d}}{.}5(\pm 0\overset{\mathrm{d}}{.}6) \times E$ valid for post-outburst data.
2. The LCs in B and V are very similar with $\langle B-V \rangle = 0\overset{\mathrm{m}}{.}564 \pm 0\overset{\mathrm{m}}{.}005$ and a standard deviation from the mean of $\sigma_{B-V} = 0\overset{\mathrm{m}}{.}091$.
3. The variations in U have a larger amplitude ($1\overset{\mathrm{m}}{.}60$) and slope of the mean brightness (10^{-4} mag/day) than in B,V ($1\overset{\mathrm{m}}{.}22$ and 7 10^{-5} mag/day, respectively).
4. The phase shifts of the minima in the U,B,V bands are within their error estimates.
5. The secondary wave with a period 553^{d} and a semi-amplitude $0\overset{\mathrm{m}}{.}077 \pm 0\overset{\mathrm{m}}{.}007$ (B) may be present.

6. Long–term variations of the brightness with a cycle length $\approx 5300^{\rm d}$ and a semiamplitude $0\overset{\rm m}{.}084 \pm 0\overset{\rm m}{.}008$ (B) is suggested.

Acknowledgements. The authors are grateful to E. Schweitzer and the observers for their contribution to the AFOEV and AAVSO databases. This work has been partially supported by VEGA grants 1282/97 and 5038/98.

References

Andronov, I.L.: 1990, *Kinem. Fiz. Nebesn. Tel* **6**, 87
Andronov, I.L.: 1994, *Odessa Astron. Publ.* **7**, 49
Andronov, I.L.: 1997, *Astron. Astrophys. Suppl.* **125**, 207
Arkhipova, V.P.: 1977, *Peremennye Zvezdy* **20**, 345
Arkhipova, V.P., Ikonnikova, N.P.: 1987, *Pisma Astron. Zh.* **15**, 140
Arkhipova, V.P., Mandel, O.E.: 1973, *Inf. Bull. Variable Stars* , No. 762
Arkhipova, V.P., Mandel, O.E.: 1991, *Pisma Astron. Zh.* **17**, 359
Bossen, H.: 1972, *Inf. Bull. Variable Stars* , No. 722
Dapergolas, A., Kontizas, E., Kontizas, M.: 1991, *Inf. Bull. Variable Stars* , No. 3583
Dumortier, B., Stram, E.: 1970, *Astronomie* **84**, 455
Gravina, R.: 1985, *Inf. Bull. Variable Stars* , No. 2834
Grygar, J., Hric, L., Chochol, D., Mammano, A.: 1979, *Bull. Astron. Inst. Czechosl.* **30**, 308
Hicks, P.D.: 1973, *Inf. Bull. Variable Stars* , 804
Hric, L., Skopal, A., Chochol, D., Komžík, R., Urban, Z., Papoušek, J., Blanco, C., Niarchos, P., Rovithis-Livaniou, H., Rovithis, P., Chinarova, L.L., Pikhun, A.I., Tsvetkova, K., Semkov, E., Velič, Z., Schweitzer, E.: 1994, *Contrib. Astron. Obs. Skalnaté Pleso* **24**, 31
Iijima, T., Mammano,A., Margoni,R.: 1981, *Astrophys. Space Sci.* **75**, 237
Kohoutek, L., Bossen, H.: 1970, *Astrophys. Lett.* **6**, 157
Munari, U., Margoni, R., Mammano, A.: 1988, *Astron. Astrophys.* **202**, 83
Mürset, U., Nussbaumer, H.: 1994, *Astron. Astrophys.* **282**, 586
Nussbaumer, H., Vogel, M.: 1991, *Astron. Astrophys.* **248**, 81
Richter, N.: 1972, *Inf. Bull. Variable Stars* , No. 708
Schild, H., Schmid, H.M.: 1997, *Astron. Astrophys.* **324**, 606
Schweitzer, E.: 1997, *ftp://cdsarc.u-strasbg.fr/pub/afoev/cyg/v1329*
Skopal, A.: 1998, *Astron. Astrophys.* **338**, 599
Skopal, A., Hric, L., Urban, Z., Pigulski, A., Blanco, C., Papoušek, J., Hanžl, D., Agerer, F., Niarchos, P., Rovithis-Livaniou, H., Rovithis, P., Tsvetkova, K., Semkov, E., Velič, Z., Michálek, F., Komačka, Ľ., Schweitzer, E., Korth, S.: 1992, *Contrib. Astron. Obs. Skalnaté Pleso* **22**, 131
Stienon, R.M., Chartrand, M.R. Shao, C.Y.: 1974, *Astron. J.* **79**, 47
Taranova, O.G., Yudin, B.F.: 1986, *Astron. Zh.* **63**, 151
Viotti, R., Hack, M.: 1993, *NASA SP* **507**, 663
Wehlau, W., Leung, K.-C.: 1964, *Astron. J.* **139**, 843
Whittaker, E., Robinson, G.: 1926, *The Calculus of Observations*, Blackies & Sons, London
Witzigmann, S., Kiehl, M., Hopp, U.: 1978, *Inf. Bull. Variable Stars* , No. 1463